ACS APPLIED MATERIALS & INTERFACES

RESEARCH ARTICLE

www.acsami.org

Synthesis of One-Dimensional Potassium Tungsten Bronze with Excellent near-Infrared Absorption Property

Chongshen Guo,*[,†] Shu Yin,[†] Lijun, Huang,[†,‡] and Tsugio Sato[†]

[†]Institute of Multidisciplinary Research for Advanced Materials, Tohoku University, 2-1-1 Katahira, Aoba-ku, Sendai, Japan

[‡]State Key Laboratory of Integrated Optoelectronics, College of Electronic Science & Engineering, Jilin University, Changchun 130012, China

ABSTRACT: Potassium tungsten oxide nanofibers were successfully synthesized via a facile hydrothermal reaction route in the presence of sulfate. After reduction under a reductive atmosphere of H_2(5 vol %)/N_2, the potassium tungsten oxide transformed to potassium tungsten bronze. Because of the lack of free electrons, the potassium tungsten oxide ($K_xWO_{3+x/2}$) showed no NIR shielding performance; however, the potassium tungsten bronze (K_xWO_3) showed promising optical characteristics such as high transmittance for visible light, as well as high shielding performance for near-infrared lights, indicating its potential application as a solar filter. Meanwhile, the potassium tungsten bronze (K_xWO_3) showed strong absorption of near-infrared light and instantaneous conversion of photoenergy to heat.

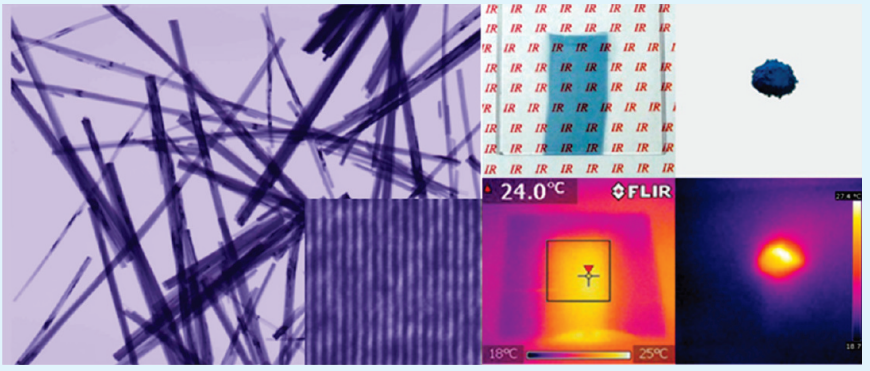

KEYWORDS: K_xWO_3, near-infrared absorption, IR shielding, tungsten bronze

1. INTRODUCTION

Tungsten bronzes (M_xWO_3) and metal tungsten oxides ($M_xWO_{3+x/2}$) with tunnel structures readily incorporate cations, such as hydrogen, lithium, etc. so that modification of host tungstate framework opens new alternatives for the synthesis of tailor-made materials.[1] Consequently, they have attracted worldwide attention in the past decades because of their unique chemical, electrochemical, and electronic properties,[2−12] which have potential applications in electronic devices, humidity and gas sensors, and secondary batteries.

Despite great structural similarities between metal tungsten oxides and tungsten bronzes, which are very difficult to be distinguished from each other only by XRD pattern, their properties are quite different. The tungsten bronzes are reduced compounds with the general formula of M_xWO_3 ($M_xW_{1-x}^{6+}W_x^{5+}O_3$). Hexagonal M_xWO_3 can be considered as a build of [WO_6] octahedral sharing corners to form a three-dimensional framework of WO_3 composition, with rather wide hexagonal tunnels in which the alkali atoms are located. The maximum alkali content for hexagonal type, $x = 0.33$, is obtained with all available tunnel positions filled. On the other hand, the general formula for the metal tungsten oxides can be written as $M_xWO_{3+x/2}$ ($M_xW^{6+}O_{3+x/2}$ or $M_xO_{x/2}\cdot WO_3$).[13] It has also been known that these metal tungsten oxides can be reduced to tungsten bronzes and, reversibly, hexagonal tungsten bronzes can be oxidized to metal tungsten oxides.[13]

In the recent years, there has been a strong desire to shield the near-infrared (NIR, wavelength of 780−2500 nm) radiation (heat rays) by employing a transparent coating on the windows of automobiles, buildings, etc.,[14] in order to reduce the energy consumption for air conditioning and thereby decrease the emission of carbon dioxide. For application as a heat ray shielding materials, excellent shielding ability of NIR rays as well as high visible light transparency is required. Recently, nanosized tungsten bronzes have been identified as materials of high interest for commercial applications involving the adsorption of near-infrared (NIR) radiation (800−2500 nm) shielding filters,[15−17] especially in comparison to current benchmark materials including lanthanum hexaboride, indium doped tin oxide, and antimony doped tin oxide.[18−20] The use of tungsten bronze nanoparticles as an additive at a very low concentration can promote the shielding performance of a clear coating, and a pigmented system can significantly reduce the power usage.[15,16]

In the present research, potassium tungsten oxide with a one-dimensional nanostructure was successfully synthesized under hydrothermal reaction conditions. The conversion of potassium tungsten oxide to tungsten bronze was performed by reducing as-obtained potassium tungsten oxide in an atmosphere of H_2(5 vol %)/N_2 at a series of temperatures for 1 h. In addition, the optical characteristic of tungsten bronze material was also carried out.

Received: May 17, 2011
Accepted: June 15, 2011
Published: June 15, 2011

2. EXPERIMENTAL SECTION

All the reagents were of analytical grade and used as received without further purification. In a typical procedure, the potassium tungsten oxide was synthesized as follows. First, K_2WO_4 and K_2SO_4 were dissolved in 50 mL of distilled water under stirring, where the concentration of K_2WO_4 and K_2SO_4 were adjusted to 0.1 and 0.2M, respectively. Then, the pHs of mixed solutions were acidified to 1, 1.5, and 2, respectively. The resultant solutions were transferred into a Teflon-lined autoclave and heated at 200 °C for 24 h. After hydrothermal reaction, the autoclaves were cooled to room temperature naturally. The products were collected by centrifugation and washed repeatedly with water and ethanol followed by drying at 60 °C in a vacuum overnight.

The potassium tungsten bronze was prepared by reducing the as-obtained potassium tungsten oxide in an H_2(5 vol %)/N_2 atmosphere at a temperature range of 400−600 °C for 1 h. In order to evaluate NIR shielding characteristics, K_xWO_3 powder was dispersed in a collodion-ethanol mixed solution at a mass ratio of ethanol: collodion: K_xWO_3 = 1.0:0.93:0.15. The coating solution was then painted on quartz glass by an applicator with a concave depth of 12.5 μm.

Characterization. The phase compositions of the samples were determined by X-ray diffraction analysis (XRD, Shimadzu XD-1) using graphite-monochromized *CuK*α radiation. The size and shape of the nanoparticles were observed by a transmission electron microscope (TEM, JEOLJEM-2010). HRTEM images and SAED images were obtained on a ZEISS LEO 922 with an accelerating voltage of 200 kV. The optical response of the coating was measured using a spectrophotometer (JASCO V-670), giving an output of transmittance in the UV, visible, and infrared ranges (200−2700 nm). Energy-dispersive X-ray spectrometer (EDS) was employed for approximate elemental analyses. The surface composition of the samples and binding energy of W_{4f} were determined by X-ray photoelectron spectroscopy (XPS, Perkin-Elmer PHI 5600). The thermogravimetric and differential thermal analyses (TG-DTA, Rigaku, TG8101D) were performed for the samples from room temperature to 900 °C with a heating rate of 10 °C/min in air.

3. RESULTS AND DISCUSSION

Figure 1 shows a typical XRD pattern of as-prepared $K_xWO_{3+x/2}$ samples synthesized at different values of pH. The reflections matched best with the hexagonal potassium tungsten oxide phase of $K_{0.33}WO_{3.165}$ (JCPDS file No.20−0940) among various tungsten oxide systems. It was found that the relative intensities of (0 0 2) diffraction peak of the product synthesized at pHs of 1.5 and 2 were stronger than those in standard JCPDS file (Figure 1b,c), indicating the preferential growth of $K_xWO_{3+x/2}$ along (0 0 2) direction. Similar results were also reported by Cao et al.[21,22] It is known that preferential growth of $K_xWO_{3+x/2}$ along (0 0 2) direction will cause sharp peak of (0 0 2). On the other hand, the $K_xWO_{3+x/2}$ of this work (x = 0.27) with fewer elemental K (compared with reference of $K_{0.33}WO_{3.165}$) in the structure also will cause shape peak of (4 0 0). It was found that the K_xWO_3, which possesses a similar structure to $K_xWO_{3+x/2}$, showed higher peak intensity of (h 0 0) around 13° with the decrement of K contents. The broadening of other peaks may be related to the weak intensities and overlapping with adjacent peaks.

The size and morphology of as-prepared samples were observed by SEM and TEM. Figure 2 presents the SEM and TEM images of $K_xWO_{3+x/2}$ synthesized at different pHs. It can be seen that the irregularly larger particles were formed at the low pH of 1 (Figure 2a,d). In contrast, the samples synthesized at pH of 1.5 and 2 exhibited a 1D fiber-like nanostructure with diameters typically in the range of 20−50 nm and lengths of about several micrometers. What is notable, further increasing

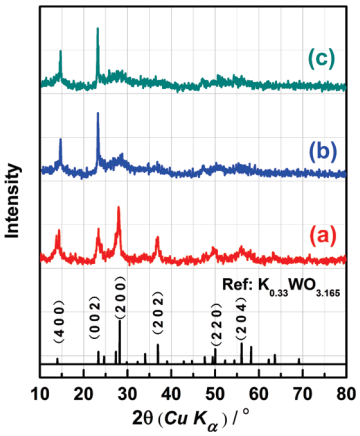

Figure 1. XRD patterns of $K_xWO_{3+x/2}$ synthesized at (a) pH 1, (b) pH 1.5, (c) pH 2.

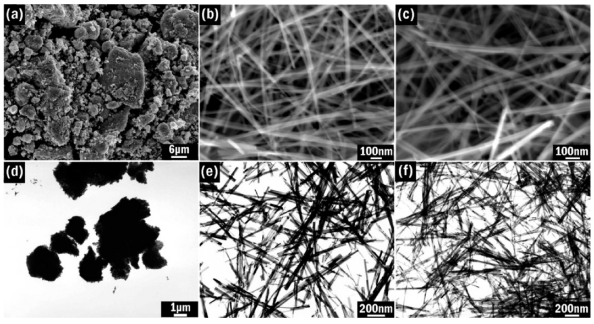

Figure 2. SEM images of $K_xWO_{3+x/2}$ synthesized at (a) pH 1, (b) pH 1.5, (c) pH 2 and (d, e) corresponding TEM images.

the initial pH of the reaction solution (pH > 2.5), there was no solid product. It is known that the $(WO_4)^{2-}$ ions condense progressively as the pH decreases.[23] From our experimental results, it is possible to suggest that the formation of irregularly larger particles is due to the high degree of condensation of tungsten species at the relative low pH. It was reported that the nanoparticles with a high aspect ratio (such as nanofibers, nanorods, nanotube, nanobelts, and so on) often show stronger intensities of specific reflections in the XRD pattern. Such a phenomenon was also observed in this work.

Figure 3 shows the HR-TEM, ED and E,DS patterns of $K_xWO_{3+x/2}$ nanofibers as-synthesized at a pH of 1.5. The $K_xWO_{3+x/2}$ with a one-dimensional hexagonal channel structure is preferential to growth along the *C*-axis and this supposition can be confirmed by the HR-TEM images (Figure 3a,b). The crystalline lattice constant along the direction of the nanofiber was calculated as 0.3768 nm, and was identified as the crystal panel of (0 0 2). Preferential growth presumption was also observed in ED analysis (Figure.3c). Both of HR-TEM and ED results were consistent with XRD measurements in Figure.1. The chemical composition analysis based on the EDS (Figure 3d) indicated the existence of K and W elements with the K/W atomic ratio of ca. 0.27.

$$K_xWO_{3+x/2} + x/2H_2 = K_xWO_3 + x/2H_2O \quad (1)$$

The conversion of $K_xWO_{3+x/2}$ to K_xWO_3 was carried out under a reductive atmosphere of H_2 (5 vol %)/N_2 at a series of temperatures for 1 h, as shown in eq 1.[13] The sample reduced at

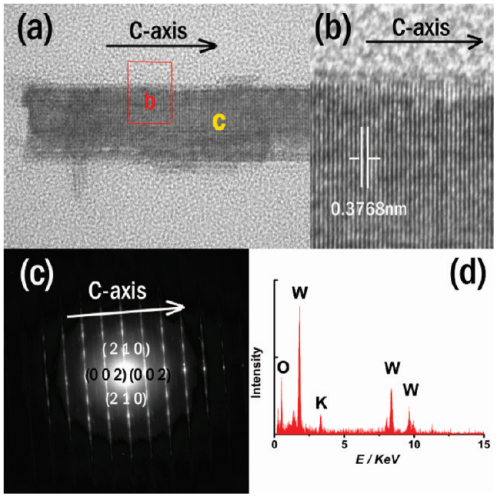

Figure 3. (a,b) HR-TEM images, (c) selected area of ED, and (d) EDS profiles of as-synthesized $K_xWO_{3+x/2}$ at pH 1.5.

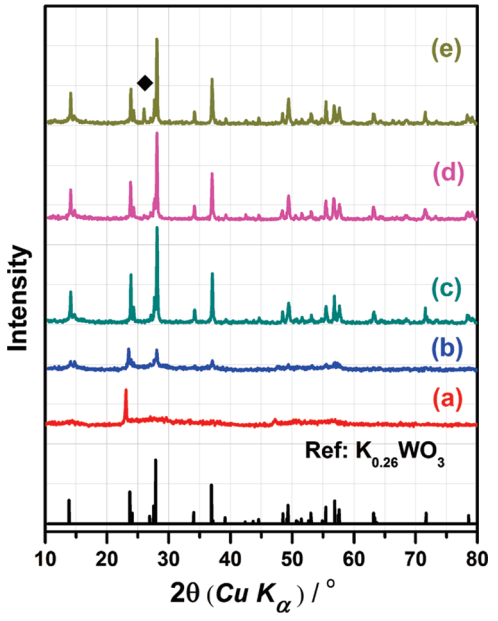

Figure 4. XRD patterns of K_xWO_3 obtained by reducing $K_xWO_{3+x/2}$ (synthesized at pH 1.5) at (a) 400, (b) 450, (c) 500, (d) 550, and (e) 600 °C under an atmosphere of H_2 (5 vol %)/N_2.

400 °C shows a very similar XRD pattern (Figure 4a) to as-synthesized $K_xWO_{3+x/2}$ (Figure 1b). In contrast, the definite pure phase of potassium tungsten bronze ($K_{0.26}WO_3$; JCPDS file No.83−1593) was observed for the samples reduced at a temperature range of 450−550 °C (Figure 4b−d). Further increasing the reduction temperature to 600 °C, the impurity of $W_{18}O_{49}$ was formed due to the deep reducing of K_xWO_3, as shown in eq 2.

$$18K_xWO_3 + (5 - 9x)H_2 = W_{18}O_{49} + 9xK_2O + (5 - 9x)H_2O \quad (2)$$

TEM images of K_xWO_3 obtained by reducing $K_xWO_{3+x/2}$ at different temperatures are shown in Figure.5. It can be seen that

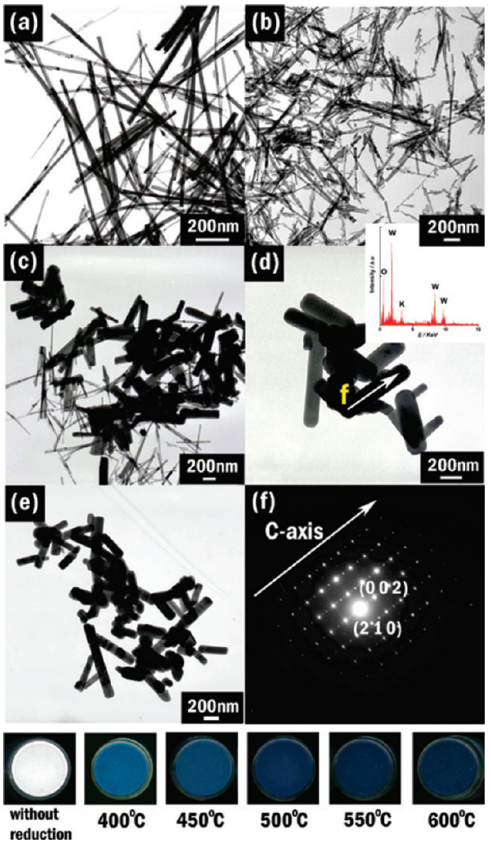

Figure 5. TEM images of K_xWO_3 obtained by reducing $K_xWO_{3+x/2}$ (synthesized at pH = 1.5) at (a) 400 °C (b) 450 °C (c) 500 °C (d) 550 °C (e) 600 °C under an atmosphere of H_2 (5 vol.%)/N_2 ; (f) the selected area of ED in (d) ; inset shows the EDS profile of (d); the blow shows the color of the samples.

the fiber-like morphology could be preserved when the reduction temperature is below 450 °C (Figure 5a,b). At a high temperature of 500−600 °C, the particles became shorter and thicker. The shrinkage of nanofibers led to the formation of nanorods (Figure 5c−e). Because of the decrement of aspect ratio from nanofiber to nanorods, the ratio of $I_{(0\ 0\ 2)}/I_{(0\ 0\ 2)}$ obviously decreased with increment of temperature (Figure 4b−e), where the $I_{(0\ 0\ 2)}$ and $I_{(0\ 0\ 2)}$ are the intensity of the diffraction peaks corresponding to crystal planes (0 0 2) and (2 0 0), respectively. The EDS analysis of the sample, shown in Figure 5d, indicated the atomic ratio of K/W was 0.26, close to the value before reduction (0.27). Such results suggest there was nearly no loss of element of K during the reducing process. ED pattern along the nanorods confirmed the preferential growth along the *C*-axis (Figure 5f). After the reduction, the white powder converted into a blue color which was originated by the chromophore of W^{5+}.

The chemical composition of the samples before and after reduction was examined by X-ray photoelectron spectroscopy (XPS). The full range of XPS spectra of $K_xWO_{3+x/2}$ and K_xWO_3 are shown in Figure 6a and Figure 6b. Peaks at binding energies corresponding to O, K and W are clearly observed, and no impurities other than carbon can be observed in the spectra. More detailed information on the chemical state of core level tungsten (W4f) was obtained from the high-resolution XPS spectra c and in Figure 6. The curves can be fitted as two spin−orbit doublets, $W4f_{7/2}$ and $W4f_{5/2}$, for the interval of about 2.1 eV. The peaks at 34.6 and 36.7 eV and

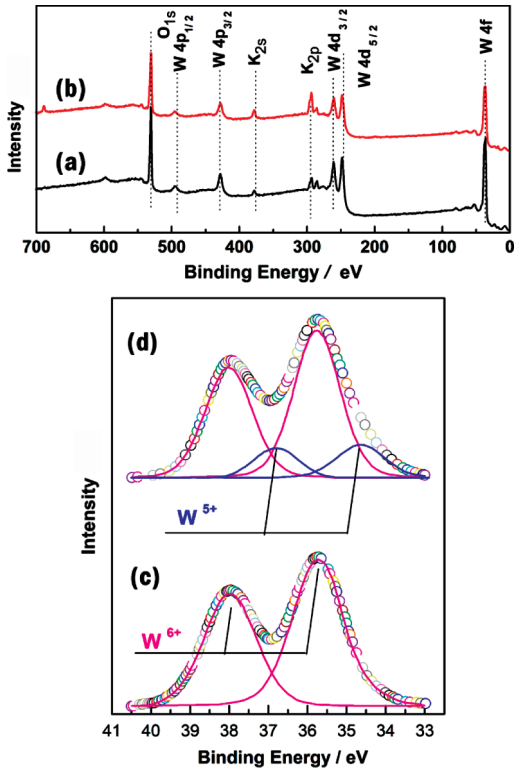

Figure 6. Full range XPS spectra of (a) $K_xWO_{3+x/2}$, (b) K_xWO_3 and W_{4f} core-level XPS spectra of (c) $K_xWO_{3+x/2}$, (d) K_xWO_3 (synthesized at pH 1.5).

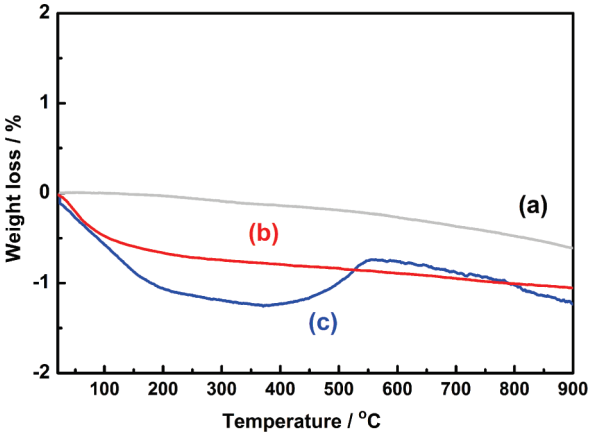

Figure 7. TG plots of (a) baseline, (b) $K_xWO_{3+x/2}$ and (c) K_xWO_3 (synthesized at pH 1.5) recorded in air with a heating rate of 10 °C/min.

35.8 and 37.9 eV were attributed to W^{5+} and W^{6+}, respectively, which agreed with the reported values.[22,24] The sample before reduction ($K_xWO_{3+x/2}$) exhibited only two peaks at 37.9 and 35.8, which are signed to W^{6+}. In contrast, the reduced sample showed mixed chemical states of W^{5+} and W^{6+}.

The thermal behavior of the samples were investigated by thermogravimetric analysis. Typical TG curves in air for the samples of $K_xWO_{3+x/2}$ and K_xWO_3 are presented in Figure.7. TG curves showed persistence of weight loss up to about 250 °C for samples, which could be due to the loss of physically or chemically absorbed water. In a temperature range of 400−550 °C, a

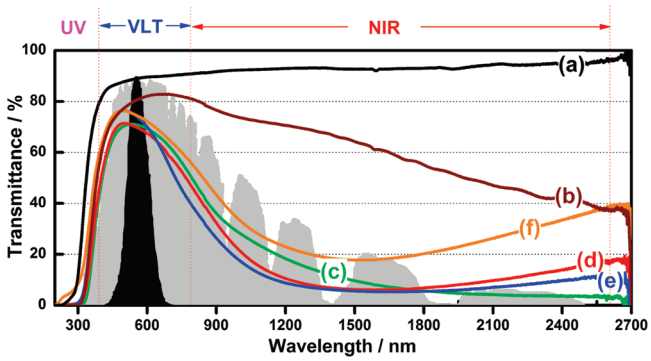

Figure 8. Transmittance spectra of (a) as-synthesized $K_xWO_{3+x/2}$ (synthesized at pH 1.5 and without reduction) and samples reduced at (b) 400, (c) 450, (d) 500, (e) 550, and (f) 600 °C under an atmosphere of H_2 (5 vol %)/N_2; The black and gray areas indicate the normalized value of the luminous efficiency function and energy wavelength distribution of the solar spectrum on the sea level.

weight gain occurred for K_xWO_3 (Figure.7c). This effect is related to the oxidation process of the potassium tungsten bronze by air oxygen, above a certain temperature, as described by eq 3. The determination of the potassium content (the value of x) is based on the TG data in the weight gain zone that is related to the bronze oxidation process.[25] In this way, the x value of K_xWO_3 was calculated as 0.251, close to the EDS result of 0.26.

$$K_xWO_3 + x/4O_2 = K_xWO_{3+x/2} \quad (3)$$

Figure 8 shows the transmittance spectra of potassium tungsten oxide ($K_xWO_{3+x/2}$) and potassium tungsten bronze (K_xWO_3) synthesized by reducing $K_xWO_{3+x/2}$ at different temperatures. Due to a lack of free electrons, the fully oxidized compound $K_xWO_{3+x/2}$ showed no NIR shielding properties and was transparent in visible and near-infrared light ranges (Figure 8a). After calcination in a reductive atmosphere, all the potassium tungsten bronze type products showed a certain degree of shielding properties in the NIR range (Figure.8b-f). It can be seen that the shielding performance of the NIR light was increased with a reduction temperature in the range of 400−550 °C, and then decreased at 600 °C. The samples K_xWO_3 reduced at 550 °C showed the best performance as solar filters, which realized high transmittance in the visible region as well as excellent shielding properties in the NIR region (Figure 8e).

When the reduction temperature is below 550 °C, it is reasonable to suggest that the reducing degree and crystallinity increases with the calcination temperature, and so the shielding performance increases with reduction temperature. On the other hand, the emergence of $W_{18}O_{49}$ impurity at high temperature inhibited the further improvement of optical properties.

Figure 9a−c shows the transmittance spectra of K_xWO_3 synthesized under different pH values followed by reduction treatment at 550 °C. The elemental analysis on the atomic K/W of sample a-c determined by EDS measurement were 0.24, 0.26, and 0.23, respectively. Previous research has found that the performance of tungsten bronze type solar filters is closely related to the morphology of the sample, and is also improved with increasing the amount of incorporated metal ions.[16] In this work, the sample synthesized under a pH of 1.5 showed high visible light transparency and stronger NIR shielding performance than those synthesized under a pH of 1 and 2 mainly due to its homogeneous rod-like morphology and high

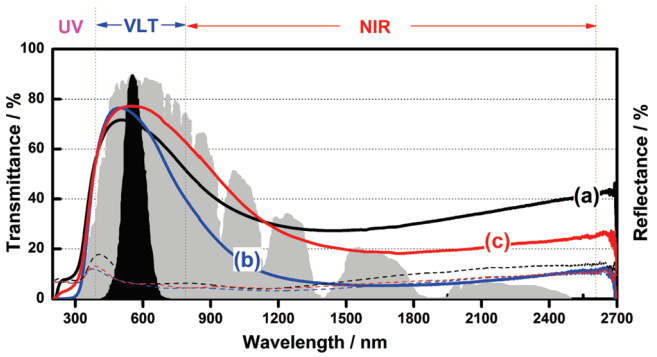

Figure 9. Transmittance (solid lines) and reflectance (dashed lines) spectra of samples synthesized at (a) pH 1 (b) pH 1.5 (c) pH 2 after reduction at 550 °C under an atmosphere of H_2 (5 vol %)/N_2; The black and gray areas indicate the normalized value of the luminous efficiency function and energy wavelength distribution of the solar spectrum at the sea level.

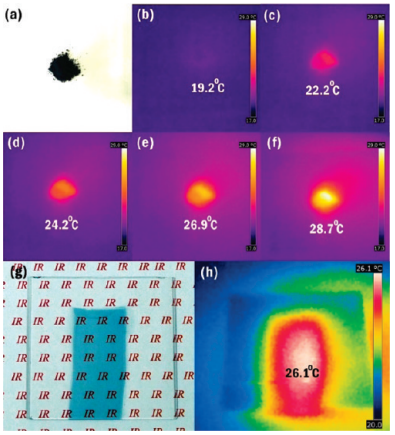

Figure 10. (a) Photograph of K_xWO_3 powder on the paper; thermographic images of K_xWO_3 powder irradiated by 50W halogen lamp for (b) 0, (c) 3, (d) 5, (e) 10, and (f) 20 s; (g) photograph of K_xWO_3 film coated on quartz glass and its (h) thermographic image after radiation for 20 s.

K/W atomic ratio (Figure 8b). The value of 100 − T(%) should be the sum of absorption (A%) and reflectance (R%) of light, where T(%) is transmittance. It can be seen that the reflectance of K_xWO_3 samples (dashed lines) were quite limited in all wavelength ranges, indicating that the shielding of NIR light by K_xWO_3 was mainly caused by the absorption of light.

Thermal results of the powder sample (Figure 10a) irradiated by 50W halogen lamp for different periods were presented in the Figure 10b−f. It can be seen that the central temperature of powder increased from room temperature of 19.2 to 28.7 °C within just 20s, whereas there was little changes on the temperature of paper background. Similar result also was observed for the K_xWO_3 contained film (Figure 10g,h). Because of strong absorption of NIR light, K_xWO_3 nanorods exhibit excellent and instantaneous conversion of photoenergy to heat.

On the basisd of the above-mentioned optical response data (Figures 8−10), it is reasonable to suggest that the KxWO$_3$ shows great potential for application as heat ray shielding materials. The simulated experiment was carried out by irradiating three sealed boxes covered by quartz glass, $Cs_{0.32}WO_3$ coated quartz glass and

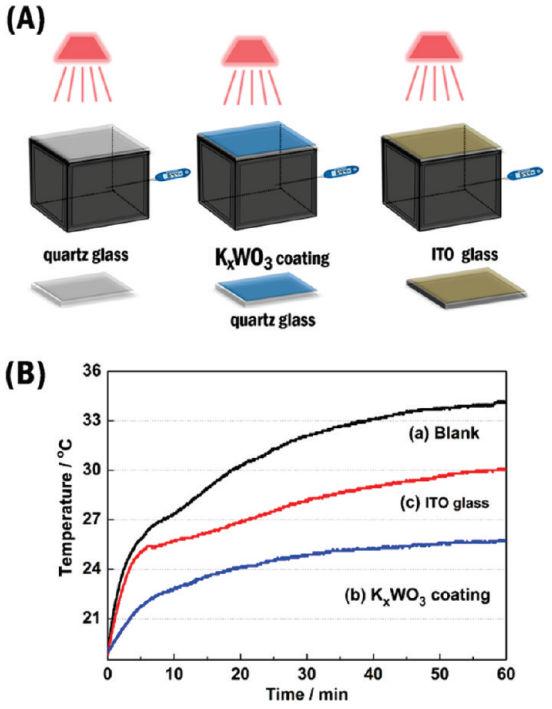

Figure 11. (A) Schematic of simulated experiment; sealed boxes with a facet covered by quartz glass, K_xWO_3 coated quartz glass and ITO glass, respectively, were irradiated by a 50w halogen lamp and the temperature changes dependent on time were recorded by an electronic thermometer. (B) Temperature dependence on irradiation time.

ITO glass, respectively, then, the temperature changes upon irradiation time were monitored. The experiment was performed at room temperature of 18 °C and a schematic of the simulated experiment is presented in Figure 11A. It can be seen that the inner temperature of the quartz glass set box increased significantly with irradiation time and reached a maximum of 34.2 °C after 1 h (Figure 11B(a)). The ITO glasses are widely used and well-known as effective infrared-ray cutoff material; however, the shielding ability of NIR of a wavelength less than 1500 nm was modest.[15,16] Although the temperature increment could be depressed by substituting quartz glass with commercial ITO glass (10 $\Omega\,\square^{-1}$), prolonged irradiation still caused the temperature to increase remarkably. In contrast, excellent heat insulating performance was realized by applying an 80% visible light transparent K_xWO_3 coating on the quartz glass. After being irradiated by a 50W halogen lamp for 1 h, the inner temperature was 25.4 °C, which was much lower than those with quartz glass or ITO covered ones.

4. CONCLUSIONS

In summary, the one-dimensional potassium tungsten oxide was successfully synthesized by hydrothermal reaction and the potassium tungsten bronze could be prepared by reducing the as-synthesized potassium tungsten oxide in H_2(5 vol %)/N_2 atmosphere. The transmittance spectra results showed that the best near-infrared shielding performance of K_xWO_3 was realized by reducing K_xWO_{3+x} synthesized under a pH of 1.5 at 550 °C. Instead of reflecting light, K_xWO_3 showed the strong absorption of near-infrared light and quick conversion of NIR lights into heat.

AUTHOR INFORMATION

Corresponding Author
*E-mail: bigguop@mail.tagen.tohoku.ac.jp. Tel & Fax +81-22-217-5597.

ACKNOWLEDGMENT

This research was supported in part by the Management Expenses Grants for National Universities Corporations from the Ministry of Education, Culture, Sports, Science for Technology of Japan (MEXT), and by the Adaptable and Seamless Technology transfer Program through target-driven R&D, JST, and Grant-in-Aid for Science Research (20360293 & 22651022).

REFERENCES

(1) Yu, A.; Kumagai, N.; Liu, Z.; Lee, Y. *J. Solid. State. Electrochem.* **1998**, *2*, 394.
(2) Raub, C.; Sweedler, A. R.; Jensen, M. A.; Broadston, S.; Matthias, B. T. *Phys. Rev. Lett.* **1964**, *13*, 746.
(3) Shanks, H. R. *Solid State Commun.* **1974**, *15*, 753.
(4) Reich, S.; Tsabba, Y. *Eur. Phys. J. B* **1999**, *9*, 1.
(5) Shengelaya, A.; Reich, S.; Tsabba, Y.; Muller, K. A. *Eur. Phys. J. B* **1999**, *12*, 13.
(6) Garif'yanov, N. N.; Vavilova, E. L. *Phys. C* **2003**, *383*, 417.
(7) Brusetti, R.; Haen, P.; Marcus, J. *Phys. Rev. B* **2002**, *65*, 144528.
(8) Leitus, G.; Cohen, H.; Reich, S. *Phys. C* **2002**, *371*, 321.
(9) Cadwell, L. H.; Morris, R. C.; Moulton, W. G. *Phys. Rev. B* **1981**, *23*, 2219.
(10) Stanley, R. K.; Morris, R. C.; Moulton, W. G. *Phys. Rev. B* **1979**, *20*, 1903.
(11) Skokan, M. R.; Moulton, W. G.; Morris, R. C. *Phys. Rev. B* **1979**, *20*, 3670.
(12) Sweedler, A. R.; Hulm, J. K.; Matthias, B. T.; Geballe, T. H. *Phys. Lett.* **1965**, *19*, 82.
(13) Hussain, A.; Kihlborg, L.; Klug, A. *J. Solid State Chem.* **1978**, *25*, 189.
(14) Hamberg, I.; Granqvist, C. G. *J. Appl. Phys.* **1986**, *60*, R123.
(15) Guo, C. S.; Yin, S.; Zhang, P. L.; Yan, M.; Adachi, K.; Chonan, T.; Sato, T. *J. Mater. Chem.* **2010**, *20*, 8227.
(16) Guo, C. S.; Yin, S.; Yan, M.; Sato, T. *J. Mater. Chem.* **2011**, *21*, 5099.
(17) Takeda, H.; Adachi, K. *J. Am. Ceram. Soc.* **2007**, *90*, 4059.
(18) Okada, M.; Yamada, Y.; Jin, P.; Tazawa, M.; Yoshimura, K. *Thin Solid Films* **2003**, *442*, 217.
(19) Elangovan, E.; Shivashankar, S. A.; Ramamurthi, K. *J. Cryst. Growth* **2005**, *276*, 215.
(20) Adachi, K.; Miratsu, M. *J. Mater. Res.* **2010**, *25*, 3.
(21) Cao, G.; Song, X.; Yu, H.; Fan, C.; Yin, Z.; Sun, S. *Mater. Res. Bull.* **2006**, *41*, 232.
(22) Gu, Z. J.; Ma, Y.; Zhai, T. Y.; Gao, B.; Yang, W. S.; Yao, J. N. *Chem.—Eur. J.* **2006**, *12*, 7717–7723.
(23) Livage, J.; Guzman, G. *Solid State Ionics* **1996**, *84*, 205.
(24) Barton, D. G.; Shtein, M.; Wilson, R. D.; Barton, D. G.; Shtein, M.; Wilson, R. D.; Soled, S. L.; Iglesia, E. *J. Phys. Chem. B* **1999**, *103*, 630.
(25) Mann, M.; Shter, G. E.; Reisner, G. M.; Grader, G. S. *J. Mater. Sci.* **2007**, *42*, 1010.

NOTE ADDED AFTER ASAP PUBLICATION

This paper was published on the Web on June 27, 2011, with the abstract graphic missing. The corrected version was reposted on June 30, 2011.